Neuron
Article

Odorant Response Properties of Individual Neurons in an Olfactory Glomerular Module

Shu Kikuta,[1,2] Max L. Fletcher,[3] Ryota Homma,[1] Tatsuya Yamasoba,[2] and Shin Nagayama[1,*]
[1]Department of Neurobiology and Anatomy, University of Texas Medical School at Houston, Houston, TX 77030, USA
[2]Department of Otolaryngology, University of Tokyo, Tokyo 113-8655, Japan
[3]Department of Anatomy and Neurobiology, University of Tennessee Health Science Center, Memphis, TN 38163, USA
*Correspondence: shin.nagayama@uth.tmc.edu
http://dx.doi.org/10.1016/j.neuron.2013.01.022

SUMMARY

Neuronal networks that are directly associated with glomeruli in the olfactory bulb are thought to comprise functional modules. However, this has not yet been experimentally proven. In this study, we explored the anatomical and functional architecture of glomerular modules using in vivo two-photon calcium imaging. Surprisingly, the deep portions of the glomerular modules showed considerable spatial overlap with other modules. Juxtaglomerular cells showed similar excitatory odorant response profiles to presynaptic olfactory sensory neuron inputs. Mitral cells exhibited a more sharply tuned molecular receptive range compared to juxtaglomerular cells, and their odorant response profiles varied depending on their interneuronal horizontal distances. These data suggest that glomerular modules are composed of functionally distinct neurons, and that homogenous odor inputs to each glomerulus may be parsed and processed in different fashions within the modules before being sent to higher olfactory centers.

INTRODUCTION

Determination of the functional significance of network modules such as columns and barrels in the mammalian brain has been an ongoing topic of research (Mountcastle, 1997). One of the primary research questions has centered around understanding the similarities and differences in the response properties of neurons within the modules (Linden and Markram, 2003). Due to difficulties in simultaneously capturing the morphologies, connectivities, and functional activities of individual neurons, it remains unclear how these neurons that are part of a module interact with each other and contribute to modular network outputs. Recent developments in optical imaging techniques have made it possible to examine this question in greater depth by allowing simultaneous observations of the activities of many cells within a single module (Ohki et al., 2005).

Olfactory sensory neurons (OSNs) that express the same type of odorant receptor converge onto either one or a few specific glomeruli in the olfactory bulb (OB), and individual odorants elicit specific spatial patterns of glomerular activity (Buck and Axel, 1991; Mombaerts et al., 1996; Mori and Sakano, 2011). Glomeruli in the OB form anatomically and functionally discrete network units that are similar to the multineuronal "barrels" and "columns" that are found in the cerebral cortex (Shepherd et al., 2004). Within each glomerulus, odor information is transferred to the various principal and local neurons that compose the glomerular module. Both types of neurons typically have only one primary dendrite that projects to a single glomerulus and receive excitatory inputs exclusively from a single type of odorant receptor. Therefore, based on the anatomical structures, all neurons in the same olfactory glomerular module would be expected to have homogenous profiles of odorant selectivity. However, these principal neurons also receive GABAergic inhibitory and other modulatory inputs from intrabulbar and/or centrifugal projections. Thus, one important question that remains to be answered is whether neurons within a single glomerular module respond to odor inputs in a homogeneous fashion. A recent study that performed dendritic recordings of projection neurons associated with a genetically identified glomerulus (using I7-M71 transgenic mice) demonstrated that the neurons comprising the associated module have similar yet slightly different odorant response profiles (Tan et al., 2010). Furthermore, simultaneous recordings of projection neurons that are associated with the same glomerulus show similar odorant selectivities but different temporal activity patterns (Dhawale et al., 2010). However, it remains unclear whether these similarities and differences in responses are associated with neuronal cell types, dendritic arborization patterns, or horizontal/vertical cell soma locations. To further understand these potential mechanisms, it is necessary to identify the anatomical and functional architecture of the glomerular modules and compare individual neuronal activities within the context of the neuronal circuits.

In the current study, we addressed these questions by visualizing the anatomical configuration of a single glomerular module in the mouse OB with calcium indicator dye labeling and in vivo two-photon imaging methods. Surprisingly, the anatomical distribution ranges of the neurons comprising the module were wider than the glomerulus, suggesting that distinct modules heavily overlap with each other. Furthermore, OSN presynaptic inputs to the glomerulus and individual postsynaptic neuronal excitatory responses were remarkably similar among cells located in the superficial bulb layer but not among those located in deeper layers. Moreover, in the deeper layers, the odorant

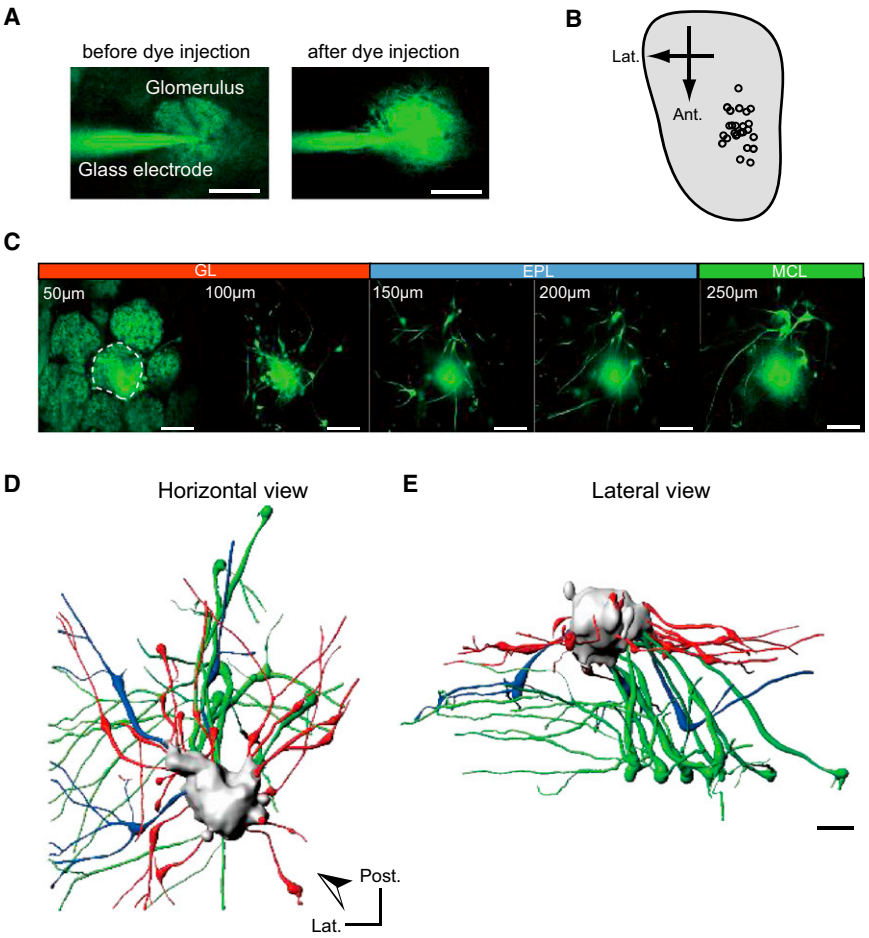

Figure 1. Multiple Neuronal Subtypes Are Associated with a Single Glomerulus

(A) Two-photon images showing the dye-filled glass pipette penetrating the target glomerulus. Images were captured before (left) and after (right) injection of electroporation dye. Glomerular formation was observed by green fluorescent spH signals.

(B) Distribution pattern of labeled glomeruli in the dorsal OB. Imaging data were collected from the anteromedial portion of the dorsal OB (also see odor-induced spH signals in Figure S1).

(C) In vivo two-photon images showing a dye-injected glomerulus and labeled neurons in different layer and depth (50–250 μm from the surface). The dye-injected glomerulus is surrounded by a dashed line. Some neurons were observed underneath the neighboring glomeruli, but these neurons were associated with the dye-injected glomerulus. The 3D reconstruction and sequential image movie of this sample are shown in (D) and (E), Figures S1C–S1E, and Movie S1.

(D and E) Horizontal (D) and lateral (E) views of 3D reconstruction of a single glomerular module (JG cells, red; tufted cells, blue; and mitral cells, green). Arrowhead (D) indicates the view angle for lateral view (E). Post., posterior; Lat., lateral.

(F) Multiple subtypes of labeled neurons were observed. Cell body locations (layers), soma shapes and sizes, and presence of L-Dends were used for grouping. Arrowheads indicate representative examples for indicated cell types. GL, glomerular layer; EPL, external plexiform layer; MCL, mitral cell layer.

Scale bars in (A) and (C–E) 50 μm, and in (F) 20 μm.

selectivities of neurons became narrower and the preferred stimuli varied depending on the locations of the neurons. These findings indicate that the response differences between these deeper neurons are location dependent.

RESULTS

Multiple Neuronal Types Associate with a Single Glomerulus

To better understand the anatomical and functional organization of a single glomerular module, we studied the anteromedial area of the dorsal OB because odorants that yield strong activation of this area have been identified (see Figure S1A available online; Uchida et al., 2000; Wachowiak and Cohen, 2001). Heterozygous knockin mice that expressed the synapto-pHluorin (spH) protein (a genetically encoded pH-sensitive fluorescent protein that reports synaptic vesicle fusion) under control of the olfactory marker protein promoter (OMP-spH mice) were used to visualize glomeruli (Bozza et al., 2004). A glass pipette filled with a calcium indicator dye (dextran-conjugated Oregon Green BAPTA-1) was guided by two-photon imaging and used to penetrate a target glomerulus. The neurons that were associated with the single glomerulus were labeled by our previously established electroporation method (Figures 1A, 1B, and S1B; Nagayama et al., 2007). Using this method, we were able to clearly visualize multiple neurons that were all associated with a single target glomerulus in the glomerular layer (GL), external plexiform layer (EPL), and even in the mitral cell layer (MCL) (Figures 1C–1F and Movie S1; 11.4 ± 1.8 cells per glomerulus, mean ± standard error of the mean [SEM]). As can be observed in Movie S1, the labeled dendrites were heterogeneous within the glomerulus and there were small parts of the glomerulus that did not appear

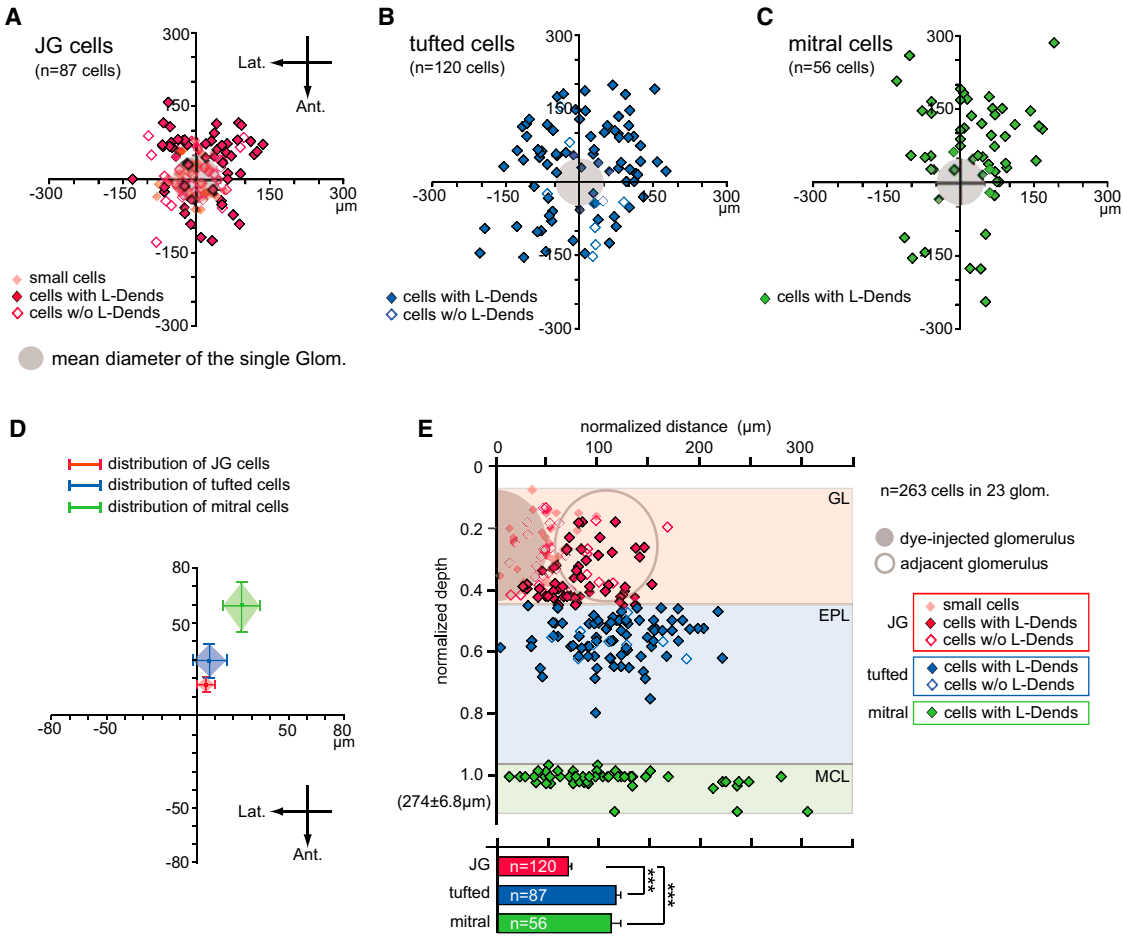

Figure 2. Distribution Patterns of Labeled Neurons

(A–C) Horizontal distribution patterns of JG cells (A), tufted cells (B), and mitral cells (C) in the dorsal OB. x-y axes indicate the anteroposterior and lateromedial axes. Filled gray circles indicate the mean size of a dye-filled glomerulus. Values on axes indicate distance from the center of the dye-injected glomerulus. Each point indicates one cell. w/o, without; Glom., glomerulus; Lat., lateral; Ant., anterior.

(D) The mean locations of each neuronal subtype from the center of the dye-injected glomerulus (red, JG cells; blue, tufted cells; green, mitral cells). The center of neuronal distributions shifted in the caudomedial direction between the GL and the MCL.

(E) Upper chart: vertical distribution patterns of labeled cells. x axis indicates the normalized distance from the center of each layer. y axis indicates the normalized depth of the labeled cells from the brain surface (0) to the MCL (1.0). Mean depth of MCL was 274 ± 6.8 μm from the OB surface. The filled gray circle indicates the presumed size of the dye-injected glomerulus, and the open gray circle represents the presumed size of the adjacent glomerulus. Each point indicates one cell. Labeled cells in the deeper layers were distributed more widely than cells in the superficial layer. Lower chart: Summary of the horizontal distribution patterns of JG, tufted, and mitral cells. Red bars, JG cells; blue bars, tufted cells; green bars, mitral cells; ***$p < 0.001$, Tukey-Kramer test. GL, glomerular layer; EPL, external plexiform layer; MCL, mitral cell layer; glom., glomerulus; w/o, without. Error bars indicate the standard error of the mean (SEM).

to be labeled. These data support the idea of anatomical compartmentalization within glomerular formations (Kasowski et al., 1999). Representative examples of glomerular structure and component neurons are shown in Figures 1D–1E. The labeled cells were grouped based on layers of soma locations, cell shapes, cell sizes, and whether lateral dendrites were present (L-Dends; Figures 1F and S1C–S1E; Table S1). Although only a small population of neurons within a glomerular module was labeled in each trial, these data enabled us to visualize the anatomical connectivity within a single glomerulus module and to compare odorant response properties between multiple neuronal subtypes associated with the same glomerulus.

Neuronal Distribution Patterns in a Glomerular Module

To investigate the anatomical architecture of a glomerular module, we first analyzed distribution patterns of cells associated with a single glomerulus (263 cells in 23 glomeruli). The labeled cells in each layer were plotted on an x-y horizontal plane that was centered on the glomerulus that had been injected with dye (Figures 2A–2C). Labeled neurons were observed in every direction from the glomerulus, and were particularly prominent in the GL and EPL. However, closer observation showed that the distribution was not isotropic, as more neurons were observed in the caudomedial area (Figure 2D). These data indicate that glomerular modules in

the dorsal OB tilt in the caudomedial direction, which is consistent with previous results (Buonviso et al., 1991). Furthermore, the distribution of neurons was wider than the sizes of their associated glomeruli.

The majority of juxtaglomerular (JG) cells in the GL (Figure 2E; 120 cells) were preferentially localized near the dye-injected glomerulus (69.0 ± 3.0 μm radius), but some of these neurons were located beneath surrounding glomeruli. Medium-sized cells with L-Dends (53 cells) were localized in the deep part of the GL. By contrast, smaller cells (30 cells) and medium-sized cells without L-Dends (37 cells) were located in the middle or superficial part of the GL (Figure S2A). These results suggest that subsets of JG cells are anatomically organized in the GL.

Relatively larger cells (>10 μm; tufted cells) were observed in the EPL (87 cells; Figures 1F and S2C), and the majority of these neurons (78 of 87 cells) had L-Dends (Figures 2B and 2E). However, there were no significant differences observed in the distribution patterns between neurons with and without L-Dends (Figure S2B). The majority of these cells were observed in the superficial portion of the EPL and were more broadly scattered than the GL cells (Figures 2B, 2E, and S2; 116.0 ± 4.8 μm radius).

In the MCL, all of the mitral cells (56 cells) possessed well-branched L-Dends (Figures 1D–1F and S2D). The majority of these neurons were located in the caudomedial direction relative to the position of their associated glomeruli (Figures 2C and 2D), and their distribution range was wider than the sizes of their associated glomeruli (Figure 2E; 111.6 ± 9.4 μm radius). It is possible that some labeled neurons were located outside the imaging field (560 × 560 μm), so we may have underestimated the distribution ranges, especially for deep mitral cell neurons. However, these data strongly suggest that EPL and MCL cell body distributions heavily overlap between neighboring glomerular modules. This overlap may increase the chance of interactions between deep neurons that are in distinct modules via reciprocal synapses with granule cells.

Direct Comparison between Presynaptic OSN and Postsynaptic Neuronal Activities

We next examined how odor information is transferred from presynaptic OSNs to postsynaptic neurons in the OB. Optical imaging experiments to determine spH signal responses to aliphatic aldehydes with different carbon chain lengths (3–9CHO) were performed using a charge-coupled device (CCD) camera. These experiments allowed us to observe OSN presynaptic activities. The target glomeruli were selected based on clear excitatory responses to the odorants, and the neurons associated with the glomerulus were then labeled with a Ca^{2+}-indicator dye. We confirmed the locations of the dye-injected glomeruli after completion of the experiments (Figure 3A). A representative example of OSN optical imaging and a labeled JG cell associated with a glomerulus are shown in Figures 3B and 3C. The presynaptic OSN and the postsynaptic neuronal calcium response traces are shown in Figures 3D and 3E. Remarkably, the response profiles of the postsynaptic neurons were similar to the profiles of the presynaptic input neurons. Molecular receptive ranges (MRRs) (Imamura et al., 1992; Mori et al., 1992) for other pairs of presynaptic nerve terminals and postsynaptic neurons are shown in Figure 3F. These responses were normalized to the strongest observed odorant-evoked response. Interestingly, clear decreases in fluorescence were sometimes observed in postsynaptic neurons (Figure 3F), but not in presynaptic OSNs. We assume that these decreases in fluorescent emissions may have resulted from inhibition of spontaneous spike discharges. Furthermore, all of the odorants that excited postsynaptic neurons also excited presynaptic OSN terminals. Although presumed inhibitory responses of postsynaptic OB neurons are not necessarily derived from presynaptic OSN activities, these results indicate that almost all of the excitatory responses observed in postsynaptic OB neurons were associated with activities of their presynaptic OSN inputs. Moreover, we did not detect significant differences in the excitatory MRR (eMRR) widths between presynaptic OSNs and postsynaptic JG cells (Figure 3G).

Sharpening of eMRR within a Single Glomerular Module

We next compared neuronal activities between different types of postsynaptic neurons within the same glomerular module (Figure 4; 124 cells in 30 glomeruli). Figures 4A and 4B shows a labeled JG cell and a labeled mitral cell with primary dendrites that belong to the same glomerulus. This JG cell showed clear excitatory Ca^{2+} responses to 5-9CHO odorant stimulations, whereas the mitral cell was only activated by 6CHO (Figure 4C). Representative MRRs for these neurons and other neurons that were in different glomerular modules are summarized in Figure 4D. Some JG cells showed only inhibitory responses to odorant stimulation. However, when we analyzed only the JG neurons that showed excitatory responses, we found that almost all odorants that activated mitral cells also activated JG cells within the same glomeruli. This relationship is summarized in Figure 4E. Furthermore, the data clearly showed that the eMRRs of deeper neurons were narrower than those of superficial cells within the same glomerular modules. These results indicate that OB circuits sharpen the odor representation within individual glomerular modules, which results in heterogeneous odor representations in different layers.

Differential Odorant Sensitivities of JG, Tufted, and Mitral Cells

It is unclear what mechanisms drive this sharp tuning of the eMRRs of deep neurons. One possibility is that the odorant sensitivities of these deep neurons may regulate the widths of the eMRRs. Early pioneer experiments suggested that tufted cells have lower thresholds for activations by OSN electrical stimulation than mitral cells (Ezeh et al., 1993; Schneider and Scott, 1983). Recently, this hypothesis was examined with odorant stimulation experiments in identical small areas in dorsal OB (Igarashi et al., 2012). However, since different glomeruli have different odorant response profiles based on their associated receptors, it has been difficult to obtain a general view of the features of different OB neuron subtypes without knowing whether the neurons belonged to same or different glomerular modules. Using our experimental procedure, we addressed this question directly by comparing neurons within the same glomerular module using various odorant concentrations (0.002%–2%). Representative examples of the images,

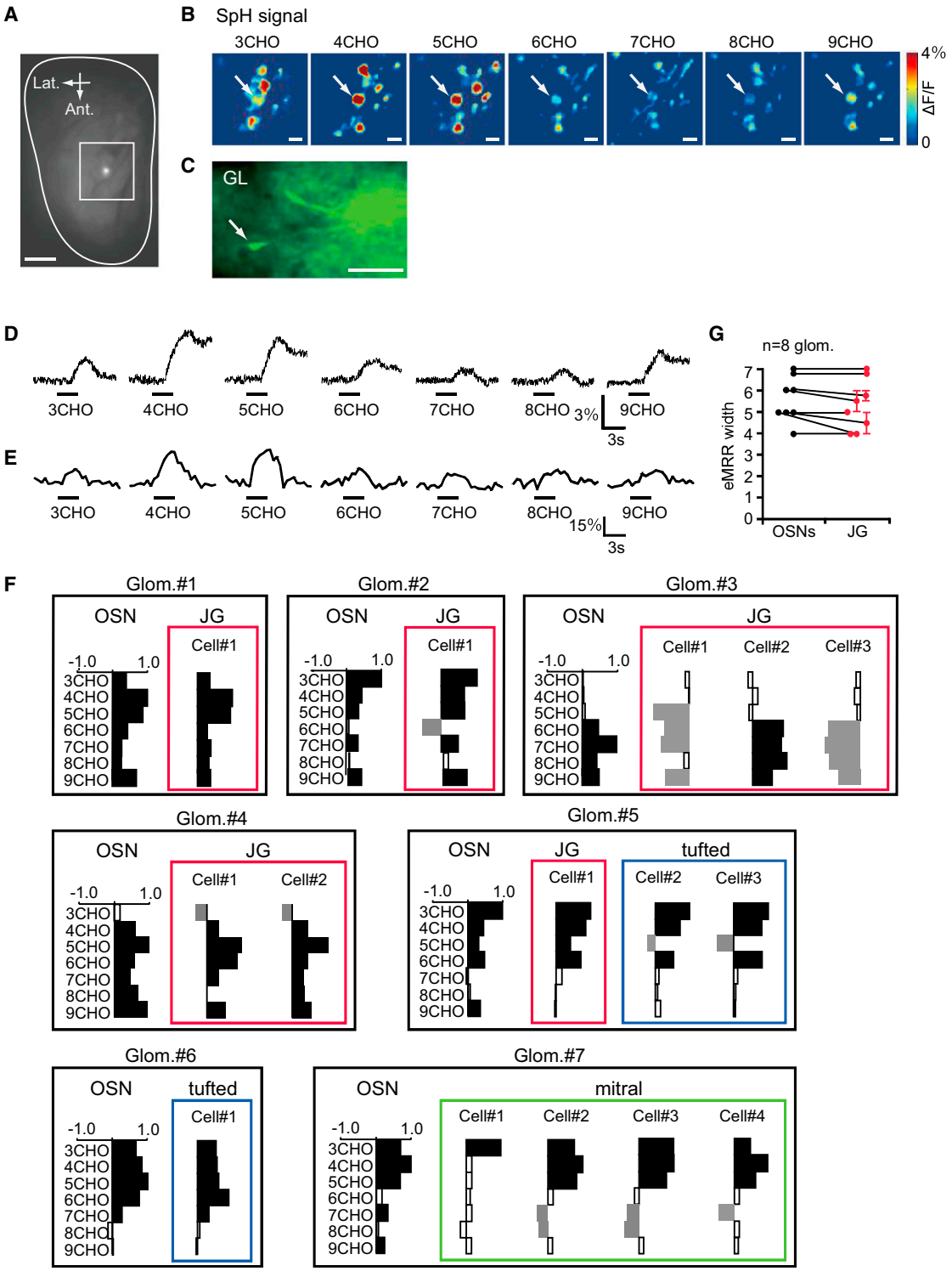

Figure 3. Direct Comparisons of Presynaptic OSN Terminal Activities and Postsynaptic Activities of Individual Cells

(A) A dye-injected glomerulus is shown (the bright spot in the center of the white square). Outline indicates the estimation of the entire dorsal OB. Ant., anterior; Lat., lateral. Scale bar: 500 μm.

(B) CCD images of odorant-evoked presynaptic spH signals around the target glomerulus. The odorants that were used to evoke signals are indicated for each image (3–9CHO). White arrows indicate the target glomeruli in which calcium indicator dye was injected after the CCD imaging experiment. SpH signals are scaled to the maximum ΔF/F (4%) in all images as indicated in the heat map on the right. Scale bar: 100 μm.

(C) In vivo two-photon image of JG cells (arrow) associated with the target glomerulus. GL, glomerular layer. Scale bar: 50 μm.

(legend continued on next page)

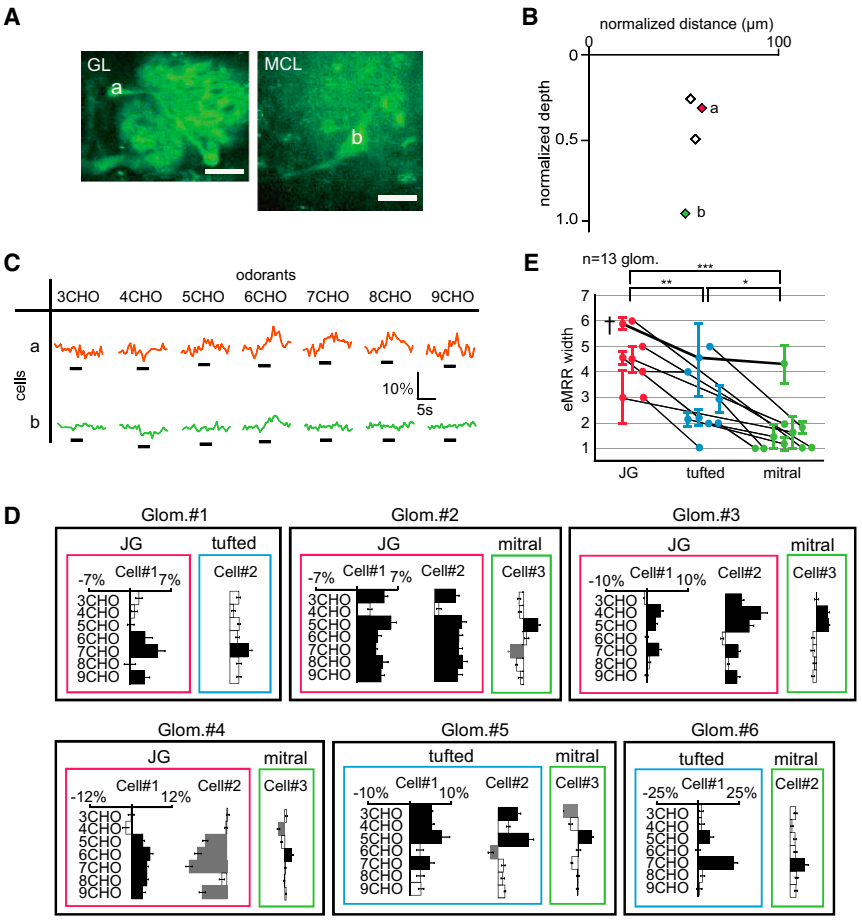

Figure 4. Odorant-Evoked Ca^{2+} Responses of Neurons in Different Layers

(A) Two-photon images of target JG (cell a) and mitral (cell b) cells associated with the same glomerulus (left image: GL; right image: MCL). Scale bars: 20 μm.

(B) Horizontal and vertical locations of labeled cells. Red (a) and green (b) diamonds correspond with the JG and mitral cells in (C), respectively. Other labeled neurons are shown as black open diamonds.

(C) Odor-evoked Ca^{2+} responses of JG (a) and mitral cells (b). Black bars under each trace indicate the timing of odor delivery (3 s). JG cell (red) showed excitatory responses with 5-9CHO stimulations, whereas the mitral cell (green) was excited by only 6CHO.

(D) MRRs of cells in different layers in other glomeruli. Bars extending right/left from the centerline indicate fluorescence increases/decreases for each cell, respectively. Cells in the same layers are surrounded with lines (red: JG cells; blue: tufted cells; green: mitral cells). x and y axes represent Ca^{2+} responses and odorants used for stimulation, respectively. JG cells had wide eMRRs while mitral cells had narrow eMRRs. Glom., glomerulus.

(E) Summary of the direct comparisons of eMRR widths within the same glomerular module. Cells associated with the same glomerulus are connected with lines (***$p < 0.001$, **$p < 0.01$, *$p < 0.05$, Steel-Dwass test, based on 14 JG, 20 tufted, and 24 mitral cells). Error bars indicate the standard error of the mean (SEM). The data sets that include all three types of neurons (JG, tufted, and mitral cells) are highlighted by a dagger mark (†) and are connected by bold lines. Glom., glomerulus.

locations, and responses of tufted and mitral cells are shown in Figures 5A–5C. Both of these representative cells showed clear excitatory responses to 2% 5CHO. Furthermore, while the tufted cell was also activated by 0.2% 5CHO, the mitral cell was not. These data provide direct evidence that mitral cells have higher odorant response thresholds than tufted cells. Other neuronal properties observed in six different glomerular modules are shown in Figure 5D. The normalized response magnitudes of individual cells were gradually decreased with decreased odorant concentrations. The minimum odorant concentration for each neuron is plotted, with neurons in the same glomerular module connected by lines, in Figure 5E. Because some neurons were activated even with the 0.002% odorant concentrations, which were the lowest used in our odorant panel, we were unable to determine accurate thresholds for these neurons. However, the results strongly suggest that JG cells are more sensitive to odorants than tufted cells and that tufted cells are more sensitive than mitral cells.

Similar Odorant Selectivities of JG Cells

To understand the odorant response profiles of neurons within the same layer, we compared excitatory odorant selectivities among JG cells in the same focal plane (Figure 6A). These JG cells (Figures 6A–6C) were characterized by relatively large cell bodies, the presence of L-Dends, and locations in the deeper portion of the GL. Although these neurons showed slightly

(D) Odorant-evoked presynaptic spH signals in the target glomerulus. The odorants that were used to evoke signals are indicated for each trace (3–9CHO). Black bars indicate timing of odorant delivery (3 s).

(E) Odorant-evoked postsynaptic Ca^{2+} signaling in JG cells. The odorants that were used to evoke signals are indicated for each trace (3–9CHO). Black bars indicate timing of odorant delivery (3 s).

(F) MRR differences between presynaptic OSNs and postsynaptic neurons in other glomeruli/neurons. Cells in the same layer are indicated (red: JG cells; blue: tufted cells; green: mitral cells). y axes: odorants used for stimulation; x axes: fluorescent changes normalized to maximum odorant responses. Bars extending right/left from the centerline indicate fluorescent increases/decreases for each cell, respectively. Filled/empty bars represent significant/non-significant responses, respectively. Glom., glomerulus.

(G) eMRR widths in presynaptic OSNs (black dots) compared to postsynaptic JG cells (red dots). Vertical axis indicates the number of excitatory odorants (eMRR widths). Glomeruli and their associated cells are connected with lines. No significant changes between OSNs and JG cells were observed (eight pairs of OSN and JG cells, $p = 0.45$, Wilcoxon t test). Error bars indicate the standard error of the mean (SEM).

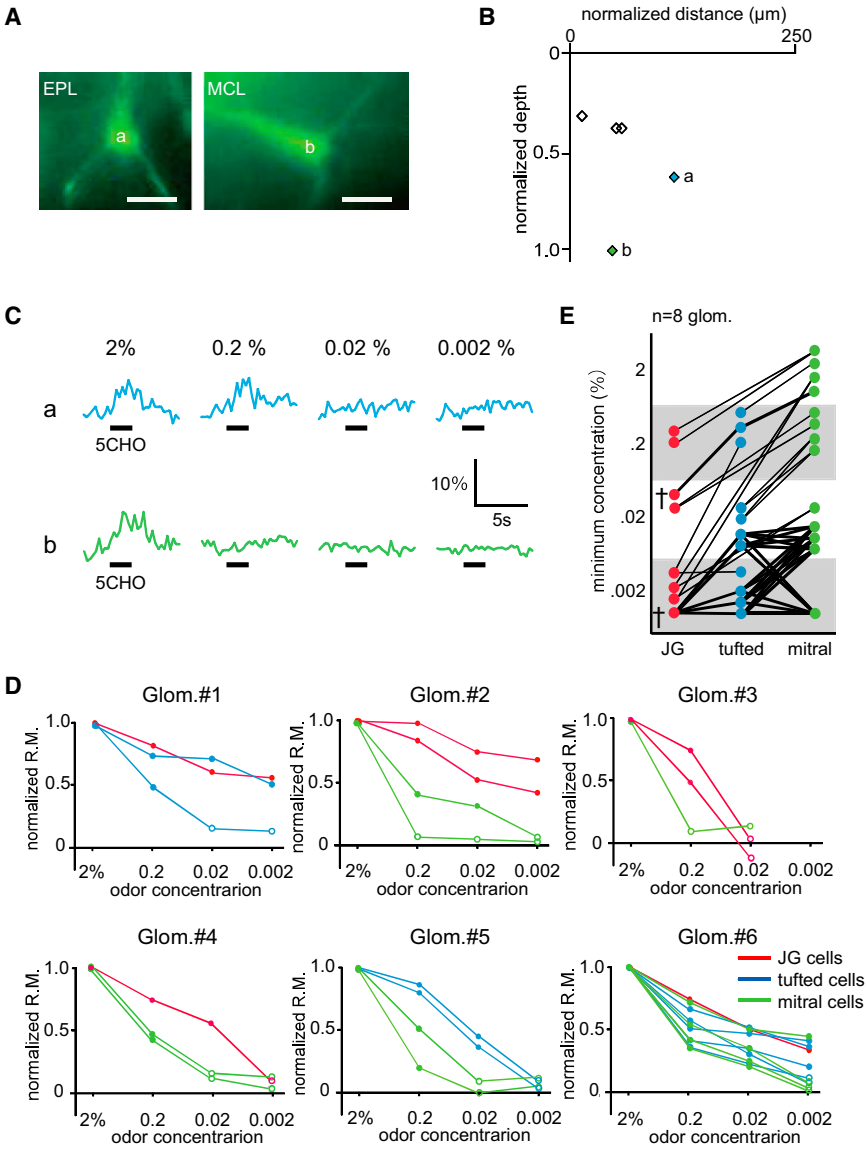

Figure 5. Differential Odorant Sensitivities of Different Neuronal Subtypes in the Same Glomerulus Module

(A) Two-photon images of tufted (a) and mitral (b) cells associated with the same glomerulus (left image, EPL; right image, MCL). Scale bars: 20 μm.

(B) Horizontal and vertical locations of labeled neurons. Blue (a) and green (b) diamonds correspond with the tufted and mitral cells in (C), respectively. Other labeled neurons are shown as black open diamonds.

(C) Odorant-evoked Ca^{2+} responses of the tufted (a) and mitral cells (b) shown in (A). Each trace indicates odor-evoked Ca^{2+} response at different concentrations of 5CHO (0.002%–2%; upper trace: tufted cell; lower trace: mitral cell). Black bar under each trace shows the timing of odor delivery (3 s).

(D) Concentration response curves for JG, tufted, and mitral cells associated with the same glomerulus (Glom. #1–6). Red, blue, and green lines indicate normalized response magnitude curves for JG, tufted, and mitral cells, respectively. Filled/empty circle points represent significant/non-significant odorant responses, respectively. Glom., glomerulus.

(E) Summary of the differential odorant sensitivities for the cell types. Each colored dot indicates the minimum concentration for inducing an excitatory odorant response in the target neurons. Neurons associated with the same glomerulus are connected with lines (eight glomeruli). The data sets that include all three types of neurons (JG, tufted, and mitral cells) are highlighted by a dagger mark (†) and are connected by bold lines. Glom., glomerulus.

different responses to 3CHO and 7CHO, the majority of the observed responses to 4–6CHO were quite similar. Summaries of the responses observed in these neurons are shown in Figure 6D. While some neurons only showed decreased fluorescent responses, the majority of JG cells in the same glomerular modules had highly similar eMRRs. Similarities in eMRRs (the ratio of the number of odorants that excited both neurons to the number of total excitatory odorants; see Experimental Procedures) between tufted and mitral cells were also compared (Figure 6E). JG cells showed higher similarities in excitatory odorant selectivities (37 pairs in nine Glomeruli; 90.3% ± 2.2%) compared to tufted and mitral cells (22 pairs of tufted cells in six Glomeruli; 64.5% ± 5.0%; 48 pairs of mitral cells in nine Glomeruli; 58.5% ± 5.0%; Steel-Dwass test, $^{**}p < 0.01$). These results indicate that JG cells in the same glomerular modules have more similar excitatory odorant selectivities than tufted and mitral cells.

Location Regulates the Odorant Response Properties of Mitral Cells

We next compared odorant responses of mitral cells in the same focal plane (Figures 7A–7C). Even though all of these neurons were associated with the same glomeruli, they showed different odorant selectivities. As shown in Figure 7C, of the four cells analyzed, cells a and b strongly responded to 6CHO and 7CHO, whereas cells c and d strongly responded to 3CHO. Interestingly, the neurons that showed similar odorant response profiles (a and b; c and d) were located in close proximities to each other within the MCL. This result suggested that neighboring mitral cells might be controlled by the same subset of granule cells. If this hypothesis is correct, then the similarities of mitral cell odorant response profiles may be related to the distance between the neurons. To test this possibility, the odorant response properties and horizontal distribution of mitral cells were analyzed (Figure 7D). These results indicate that neighboring pairs of mitral cells had high odorant response similarities and that distant pairs had lower similarities. This relationship is summarized in Figure 7E. The similarities of odorant selectivities significantly correlated with the intercellular distances between mitral cells (48 pairs of mitral cells in

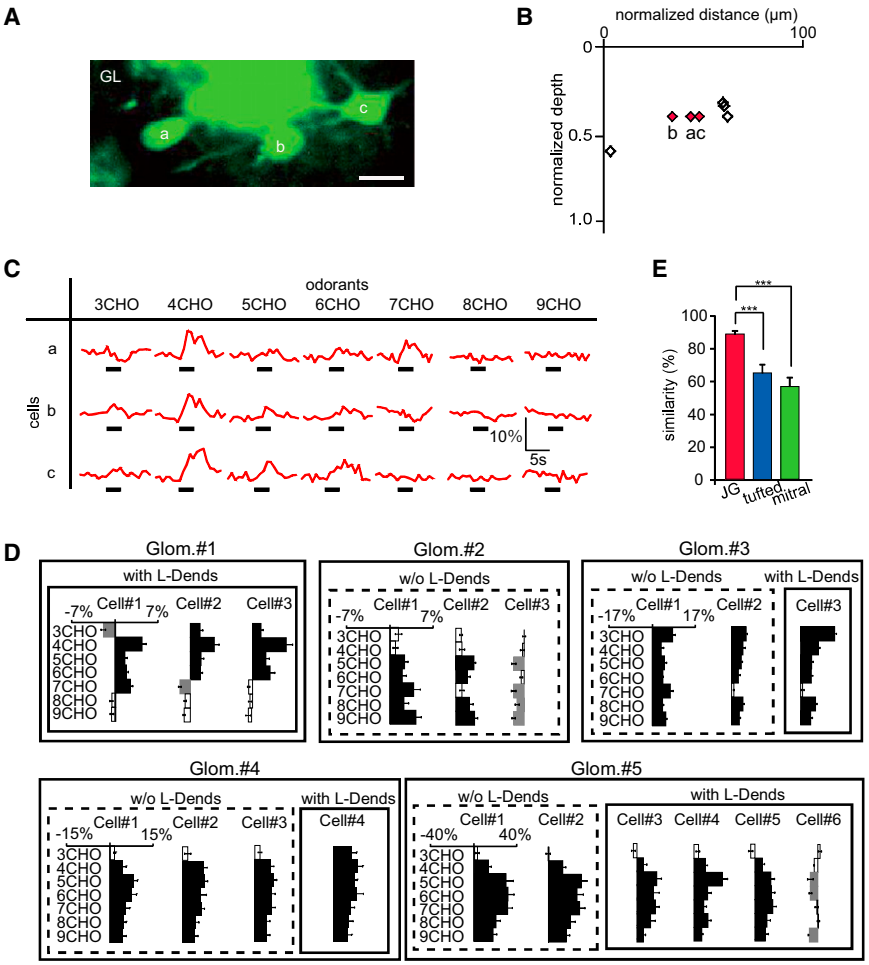

Figure 6. Excitatory Odorant Selectivities of JG Cells

(A) Two-photon image showing three JG cells in the same focal plane. Scale bar: 20 μm.

(B) Horizontal and vertical locations of the labeled JG cells. Red diamonds (a–c) correspond with the neurons in (C). Other labeled neurons are shown as black open diamonds.

(C) Odor-evoked Ca^{2+} responses for the three indicated JG cells in (A) and (B). Black bars under each trace show the timing of odor delivery (3 s). All of these neurons show similar excitatory odorant response profiles.

(D) MRRs for JG cells in (a–c) (Glom. #1) and other glomeruli. JG cells with and without L-Dends are surrounded by solid and broken outlines, respectively. x and y axes represent Ca^{2+} responses and odorants used for stimulation, respectively. Bars extending right/left from the centerline indicate fluorescent increases/decreases for each cell, respectively. Glom., glomerulus.

(E) Summary of the similarities in excitatory odorant selectivities of JG, tufted, and mitral cells. JG cells show significantly higher similarities in odorant selectivity than tufted and mitral cells (***$p < 0.001$, Steel-Dwass test, based on 40 JG, 22 tufted, and 48 mitral cell pairs). Red bar, JG cell pairs; blue bar, tufted cell pairs; green bar, mitral cell pairs. Error bars indicate the standard error of the mean (SEM).

nine glomeruli, $R = -0.76$, $p < 0.01$). By contrast, the similarities of odorant selectivities in JG cells were not correlated with interneuronal distances (Figure 7F; 37 pairs of JG cells in 11 glomeruli, $R = 0.05$, $p = 0.76$). Furthermore, the similarity of excitatory/inhibitory responses was also analyzed using correlation coefficient and cosine similarity as similarity metrics (Figures 7G, 7H, and S3; see Experimental Procedures). In both analyses, the similarity of mitral cell pairs demonstrated significant negative correlation with interneuronal distance (Figure 7G; Pearson's correlation coefficient, $R = -0.77$, $p < 0.001$) (Figure S3A; cosine similarity, $R = -0.66$, $p < 0.001$), whereas that of JG cell pairs had lower correlations (Figure 7H; Pearson's correlation coefficient, $R = 0.01$, $p = 0.93$) (Figure S3B; cosine similarity, $R = 0.24$, $p = 0.13$). Interestingly, the values of correlation coefficients and cosine similarity were not always high. This observation suggests that the difference in response similarity of mitral cells is more likely accounted for by a difference in the overall shape of response profile (e.g. optimal stimulus) than by a difference of the threshold that is applied to the otherwise similar response profile. In addition, if we focus solely on the neighboring mitral cell pairs (within 50 μm), the mean Pearson's correlation coefficient is $R = 0.86$ ($n = 17$ pairs), which is apparently higher than the corresponding value in a previous report ($R = 0.68$; Dhawale et al., 2010). However, it remains unclear whether the response profile in our study is indeed less divergent, taking into account that the smaller number of odorants in our study might limit the precision of the estimate of correlation coefficients and make such a comparison difficult. However, overall, these results suggest that interneuronal distances regulate the generation of differential odorant selectivities in mitral cells but not in JG cells.

DISCUSSION

Odor Processing in Glomerular Modules

In this study, we successfully compared the odorant response properties of neurons within individual glomerular modules. Overall, we found that odor selectivities are sharpened in a gradient from superficial neurons to deep layer neurons, as shown in Figure 8. The schematic model proposed in Figure 8 is based on the lateral inhibition hypothesis that mitral cell activities are dependent on both the summation of the excitatory inputs from their own glomeruli and inhibitory inputs from granule cells that reflect the activities of multiple surrounding glomeruli with slightly different MRRs (Yokoi et al., 1995). In this schema, multiple odorant information (shown as different colored circles) is transferred from presynaptic OSN to postsynaptic neurons within a glomerular module. JG cells have wide excitatory odorant selectivities that are similar to those of presynaptic

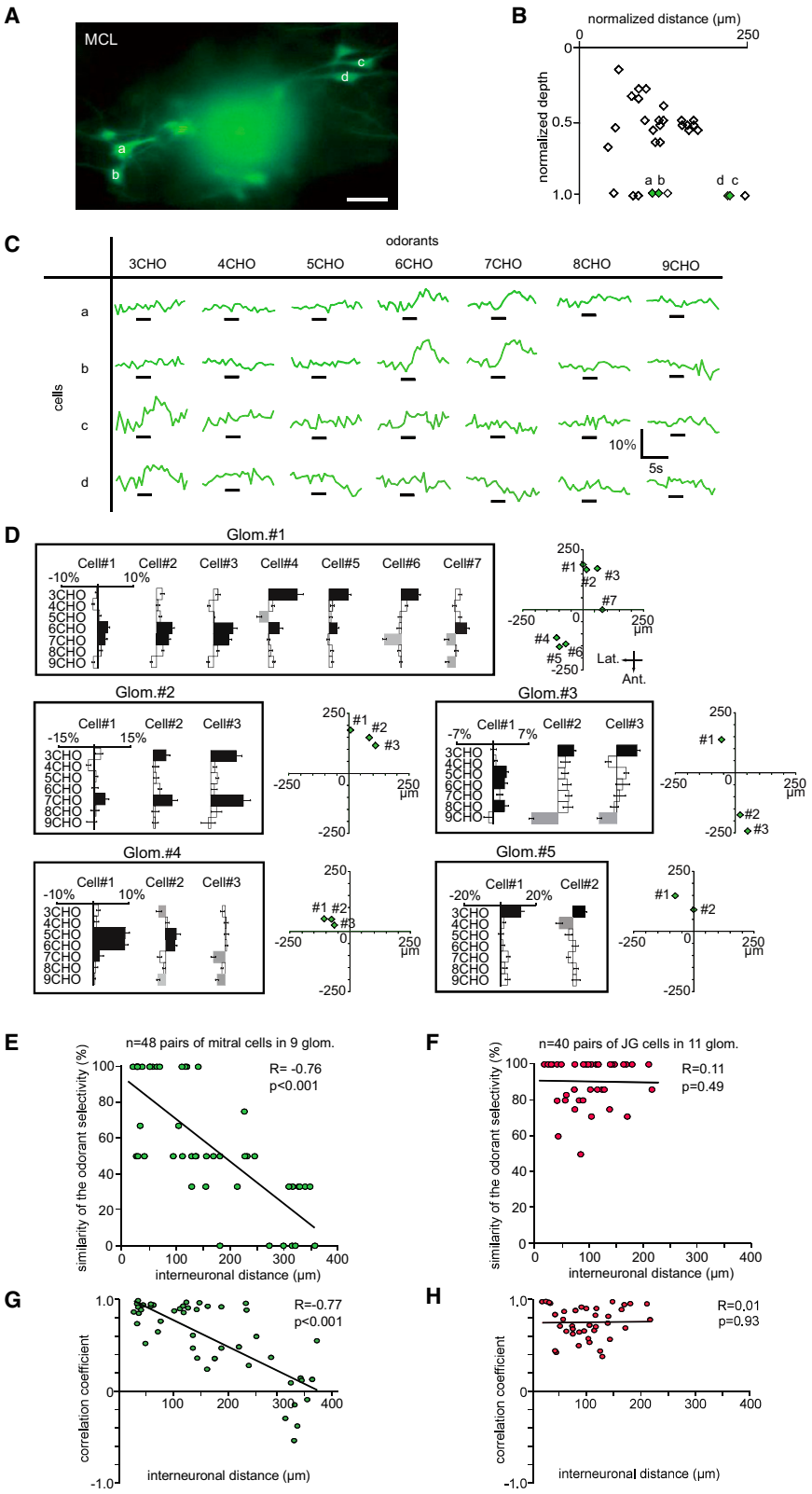

Figure 7. Excitatory Odorant Selectivities of Mitral Cells

(A) Two-photon image of mitral cells associated with the same glomerulus on bottom left (cells a and b) and upper right (cells c and d). Scale bar: 50 μm.

(B) Horizontal and vertical locations of labeled neurons. Green diamonds (a–d) correspond with neurons in (C). Other labeled neurons are shown as black open diamonds.

(C) Odor-evoked Ca^{2+} responses for cells in (A) and (B). Black bar under each trace indicates timing of odor delivery (3 s). Mitral cells a and b show strong responses to 6–7CHO stimulation and similar excitatory odorant selectivities. Cells c and d showed excitatory responses to 3CHO stimulation. The glomerulus associated with all the cells in (a) was activated by 3–7CHO odorants (Figure 3F; Glom. #6).

(D) MRRs for mitral cells associated with the same glomeruli and their horizontal distribution patterns. Cells surrounded by lines originate from the same glomerulus. x and y axes represent Ca^{2+} responses and odorants used for stimulation, respectively. Bars extending right/left from the centerline indicate fluorescent increases/decreases for each cell, respectively. The horizontal distribution patterns for the cells are shown in the charts to the right of the indicated glomeruli. x and y axes for the horizontal plots indicate the lateromedial and anteroposterior axes. The center points for the horizontal plots indicate the centers of the dye-injected glomeruli. Error bars indicate the standard error of the mean (SEM).

(E and F) Correlations of interneuronal distances and the similarity of excitatory odorant selectivities between mitral (E) and JG cells (F).

(G and H) Correlation coefficient-based analysis between odor-induced fluorescent changes (increase/decrease) and interneuronal distances for each pair of mitral (G) and JG cells (H) (mitral cells: $R = -0.77$, $p < 0.001$; JG cells: $R = 0.01$, $p = 0.93$). Each dot indicates mitral (E and G) or JG (F and H) cell pairs. Adjacent pairs of mitral cells show similar odorant selectivities, while separated pairs do not (48 pairs, $R = -0.76$, $p < 0.001$). By contrast, interneuronal distances of JG cells did not correlate with excitatory odorant selectivities (40 pairs, $R = 0.11$, $p = 0.49$).

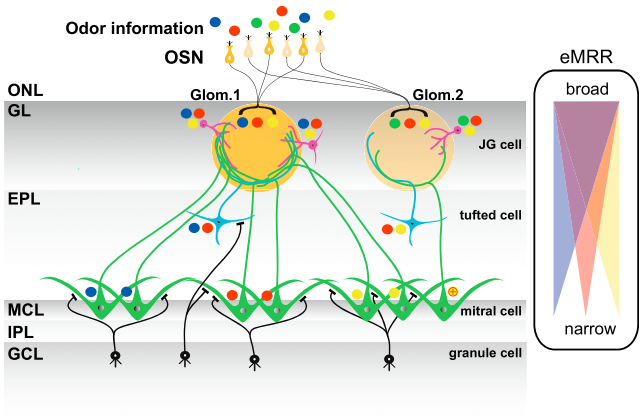

Figure 8. Schematic Diagram of Odorant Representations in Multiple Neurons of a Glomerular Module

Each colored circle represents distinct odorant (blue, red, green, yellow). In this model, OSN and JG cells handle three odorants information, while tufted cells handle two, and mitral cells handle one. The odorant tuning specificities of the mitral cells depend on the locations of the cell bodies. Neighboring mitral cells likely receive similar inhibitory control from the same subset of granule cells. Thus, neighboring mitral cells may show similar odorant responses profiles while distant mitral cells show different ones. However, if neighboring mitral cells receive excitatory inputs from different glomeruli (⊕ mitral cell), their odorant selectivities would due to disparate excitatory inputs from their associating glomeruli. Right: schematic diagram of eMRR sharpening. From the GL to the MCL, eMRR widths become more narrowly tuned. However, the preferred odorants resulting from the narrowed tuning differ depending on the location of each neuron. OSN, olfactory sensory neuron; ONL, olfactory nerve layer; GL, glomerular layer; EPL, external plexiform layer; MCL, mitral cell layer; IPL, internal plexiform layer; GCL, granule cell layer; Glom., glomerulus; JG cell, juxtaglomerular cell.

OSNs. Tufted cells are activated by a part of the whole input to the glomerulus and, as a result, show narrower odorant selectivities. Mitral cells show the most narrowly tuned odorant selectivities. Furthermore, neighboring mitral cells are likely subjected to inhibitory control by the same subset of granule cells (Buonviso et al., 1996) and have similar odor selectivities, whereas distal pairs of mitral cells that are controlled by different subsets of granule cells have different odor selectivities. This model supports the hypothesis that odor information is sharply and heterogeneously tuned by different projection neurons, even if they are in the same glomerular module. Furthermore, the separately locating projection neurons send subdivided information of a glomerular input and, as a consequence, OB send a large number of differential olfactory information channels to higher olfactory centers (Tan et al., 2010). Without accurate identification of the neurons that were recorded and the glomerular module structures, it is extremely difficult to determine similarities in odorant response profiles between neighboring mitral cells. Because of these difficulties, some studies have reported controversial results (Buonviso et al., 1992; Egaña et al., 2005).

The morphological, structural, and functional properties of the granule cells are critical factors in this model. The apical dendrites of typical granule cells branch and extend into a narrow area of the EPL (50–200 μm) (Orona et al., 1984; Shepherd et al., 2004). Moreover, reciprocal synapses that contact within 150 μm of the perisomatic regions of mitral cells suppress somatic spikes and result in the failure of axonal outputs (Lowe, 2002). This suggests that lateral inhibitory effects occur within a small local area. In addition, distinct granule cell subtypes have variable dendritic branching patterns and connections within the EPL (Imamura et al., 2006; Mori et al., 1983; Naritsuka et al., 2009; Orona et al., 1983). Tufted and mitral cells may therefore be differentially regulated by microcircuits that contain distinct granule cell subtypes (Ezeh et al., 1993; Imamura et al., 2006; Macrides et al., 1985; Orona et al., 1983). This implies that distinct subsets of granule cells mediate differential inhibitory control even within a single glomerular module, and may create layer-specific odorant response properties. These different layers would then send the varied aspects of odorant information to different higher brain center areas in different manners. This has indeed been suggested to be the case for mitral and tufted cells (Fukunaga et al., 2012; Griff et al., 2008; Igarashi et al., 2012; Nagayama et al., 2010; Nagayama et al., 2004).

Potential Mechanisms that Tune Odorant Selectivity within the Glomerular Module

Lateral inhibition is one of several possible neuronal mechanisms that may contribute to the phenomenon of odor selective tuning. Another possibility may be the differential input sensitivities of each cell type, as the cells show differences in their sizes, morphologies, and distances from the glomeruli (Figures 5, S2C, and S2D). JG cells are relatively smaller and may have weaker attenuation of dendritic excitatory postsynaptic potentials due to higher input resistances, different lateral inhibitory connections, and short pathways between the excitatory inputs and the cell body. Mitral cells may require larger excitatory postsynaptic potentials for activation than JG and tufted cells and may only deal with odor information from odorants present at relatively high concentrations. These higher thresholds for the activation of mitral cells could result in more finely tuned odorant selectivities. This idea may answer how sharpening occurs, but does not explain why deeper neurons show differential odor selectivities in an interneuronal distance-dependent manner.

Another possible mechanism is functional compartmentalization within a glomerular formation. Previous morphological and immunohistochemical findings suggest that the axonal and dendritic arborizations within glomeruli are not evenly distributed (Hálasz and Greer, 1993; Kasowski et al., 1999). Furthermore, a functional study suggested that odorant stimulations do not evenly activate olfactory sensory nerve terminals within a glomerulus (Wachowiak et al., 2004). Because we observed that similarities in odorant selectivities were not associated with interneuronal distances in the GL (Figures 7 and S3), it is reasonable to speculate that this differential tuning effect is largely controlled in a deeper part of the OB. Therefore, although we cannot neglect the potential contributions of multiple factors, we currently favor the lateral inhibition hypothesis in which mitral-granule cell circuits drive the heterogeneous odorant selectivities of deeper layer cells.

Inhibitory Response and Temporal Dynamics

Multiple neuronal subtypes have been identified recently within the GL (Aungst et al., 2003; Kiyokage et al., 2010; Kosaka

et al., 1998; Liu and Shipley, 2008) and are thought to play different functional roles (Shepherd et al., 2004; Shipley and Ennis, 1996). However, we did not observe clear differences in excitatory responses among GL neuron subtypes. One reason may be that it is difficult to detect inhibitory responses with calcium imaging. However, we were able to detect odor-induced decreases in fluorescent responses. In fact, when we analyzed the potential inhibitory responses indicated by decreased fluorescence (Charpak et al., 2001; Sachse and Galizia, 2002), the data showed an interesting trend. Individual JG cells without L-Dends showed either excitatory or presumed inhibitory responses to odorant stimulation, but not both, while JG cells with L-Dends, tufted cells and mitral cells frequently showed a combination of excitatory and presumed inhibitory responses (Figure S4). These data imply that neurons without L-Dends have less varied functional roles compared to neurons with L-Dends, and provide evidence for functional differences between these neurons. Therefore, distinct functional responses to inhibitory inputs might be critical properties of OB neurons.

Another potential reason for the difficulties in finding subtype specific functional roles may be the slow acquisition rate of two-photon imaging. Since the temporal accuracy of spike discharges on respiratory rhythms is thought to contribute to odor information coding (Carey and Wachowiak, 2011; Cury and Uchida, 2010; Kepecs et al., 2006; Phillips et al., 2012; Shusterman et al., 2011; Smear et al., 2011; Uchida et al., 2006; Wachowiak, 2011), it may be worthwhile investigating the temporal activity patterns of individual neurons in the same module. Electrophysiological experiments performed in acute OB slices revealed that external tufted cells create oscillatory phasic network activities within a glomerulus (Hayar et al., 2004; Liu and Shipley, 2008), and glutamate spillover and gap junctions within the glomerulus contribute to synchronous neuronal activities within a glomerular module (Christie et al., 2005; Ma and Lowe, 2010; Schoppa and Westbrook, 2001, 2002). Those results imply that a glomerulus may be a functional unit that creates a temporal clock of synchronized activities. Moreover, recent research showed that neurons in the same glomerular module are activated in different phases of respiratory rhythms (Dhawale et al., 2010). However, most current two-photon imaging methods do not have enough speed to measure temporal activity patterns. In addition, we cannot rule out the possibility of nonlinearity in calcium signals and a potentially high threshold in the calcium imaging method. These drawbacks of the imaging technique might cause distortions of response profiles and make the data difficult to compare directly with electrophysiological experimental data. However, a recently developed high-speed two-photon imaging system (Grewe et al., 2010; Zeng et al., 2006) and voltage-sensitive protein sensor (Jin et al., 2012) might help overcome this problem. Indeed, the temporal dynamics of different cell types may be revealed in the future via these new imaging and electrophysiological techniques. Such experiments could help further the understanding of odor information coding at the network level.

Circuitry Organization in the OB

Recent anatomical and physiological research has reported horizontal inhibitory interactions by short axon cells in the GL and the segregation of lateral inhibitory systems in the GL and EPL (Aungst et al., 2003; Kiyokage et al., 2010). Although not yet experimentally confirmed, these distinct horizontal inhibitory systems in different layers may contribute to the differential activities of JG and mitral/tufted cells within the module. If a glomerulus is a functional unit to coordinate temporal spike activities of component neurons, the short axon cells may regulate the rhythmic clock of their own glomerulus relative to the clocks of surrounding glomeruli by the horizontal interaction in GL. Therefore, it will be important to determine whether short axon cells show spike discharges that are synchronized with other component neurons in the same glomerular module and how the surrounding glomerular neurons use this spike timing information.

A tracing study that used a *trans*-synaptic virus found a cylindrical columnar structure composed of subsets of granule cells in the OB (Kim et al., 2011; Willhite et al., 2006). Interestingly, the size of this structure is similar to the size of a glomerulus. However, the glomerular module does not appear to have this columnar structure (Figure 2), suggesting that these columns of granule cells may not be directly associated with the glomerular module. One possibility is that these granule cell columns may instead be modules that control the projection neuron activities of the OB. This hypothesis would explain why the mitral cells in this study showed different activities depending on their locations. The neighboring mitral cells, which showed similar odorant response properties, may have belonged to the same granule cell control modules. While very little is known about these subset-based structures and connectivities (Eyre et al., 2008), an interesting hypothesis is that the OB is composed of multiple functional/anatomical network modules that consist of distinct cell subtypes and that process odorant information in multiple dimensions within a restricted spatial structure. Furthermore, research into individual neuronal activity patterns will help determine the horizontal and vertical anatomical structures and aid the understanding of odor processing mechanisms in glomerular modules and the entire OB.

EXPERIMENTAL PROCEDURES

Animal Preparation

The Animal Welfare Committee of the University of Texas Medical School at Houston approved all experimental protocols in accordance with the guidelines of the National Institutes of Health. A total of 32 adult mice (6–24 weeks old, heterozygous OMP-Synapto-pHluorin knockin mice, Jackson Laboratories) were anesthetized with urethane (1.2 g/kg, intraperitoneal [i.p.]). Mannitol (1.0 g/kg, i.p.) was used to reduce intracranial pressure. The animals were kept on a heating pad with circulating water at 40°C throughout the procedures. The bone covering the dorsal OB was carefully drilled and thinned with a dental drill. In some experiments, 1.5% agar dissolved in Ringer's solution (140 mM NaCl, 5 mM KCl, 1 mM $MgCl_2$, 2 mM $CaCl_2$, 0.01 mM EDTA, 10 mM HEPES and 10 mM Glucose; pH 7.5) was applied to reduce brain pulsation.

Electroporation

Dextran-conjugated Oregon Green BAPTA-1 (Invitrogen) was diluted in Ringer's solution and used at a final concentration of 10%–20%. Glomeruli in OMP-spH knockin mice were visualized by two-photon fluorescence imaging (Bozza et al., 2004), and a dye-filled glass pipette (tip I.D., 2.5 μm) was inserted into the center of the target glomerulus.

Small square pulses were delivered from a current isolator (2 Hz for 2–10 min). The pulses were transferred to pseudoexponential waveforms by

a capacitor (2350 pF) that bridged the outputs of the isolator (Figure S1). The waveforms were composed of sharp currents (5–10 μA amplitude, 1–2 ms duration) that were followed by small tail currents ($\tau \approx 25$ ms). As previously reported, this electroporation method was effective within a 20–30 μm diameter and adequately labeled single glomerular-specific cells in the OB (Nagayama et al., 2007).

Odorant Presentation

A combination of liquid-dilution and flow-dilution methods was used for dilution of odors. Odorants were first diluted in mineral oil to 0.01%–10% in glass tubes. Filtered nitrogen was used as the odor vapor carrier to avoid oxidation. The saturated vapor for each odorant was then diluted fivefold through mixture with pure air. The final concentrations were adjusted to 0.002%–2% with two separate mass flow controllers for clean air and odor vapor. The total airflow was fixed at 0.5 l/min throughout the experiment. To avoid cross-contamination, multiple Teflon tubes were used for different odorants that were delivered in parallel. One suction tube and multiple odor delivery tubes were banded and then placed in front of the nostrils of the mice. To deliver odorants, the suction was stopped with a solenoid valve, and the diluted odorants were blown toward the nostrils from a distance of 1 cm. The odorants were usually presented for 3 s and with an interstimulus interval of more than 60 s to avoid potential sensory adaptations. A constant vacuum pipe was placed over the heads of the mice for quick exhaustion of the odorants. A homologous series of aliphatic aldehydes with different carbon chain lengths were used (propylaldehyde [3CHO], butylaldehyde [4CHO], valeraldehyde [5CHO], hexylaldehyde [6CHO], heptylaldehyde [7CHO], octylaldehyde [8CHO], nonylaldehyde [9CHO]) to stimulate the olfactory epithelium.

Classification of Cells and Layers

The three layers in the OB were distinguished based on anatomical features. The glomerular layer (GL) was identified by the glomerular spH image and an expected thickness of 100–150 μm from the surface of OB. At a depth of 250–350 μm, neurons with large cell bodies and well-branched L-Dends were nearly arranged in a single focal plane. This layer was defined as the mitral cell layer (MCL). In some preparations, mitral cells were confirmed by histology (data not shown). The layer that was intermediate to the GL and MCL was defined as the external plexiform layer (EPL; depth 100–250 μm). The depths of individual neurons were normalized to the depths of the mitral cell layer for each sample, with, the brain surface defined as 0.0 and the MCL as 1.0. Based on the cell layers, cell sizes, cell shapes, and the presence or absence of L-Dends, labeled neurons were categorized into six neuronal subtypes (Table S1).

Three cell subtypes were distinguished in the GL based on morphological structures (Figure 1 and Table S1). Small cells (n = 30) did not have L-Dends and were assumed to be periglomerular cells. The middle cells with/without L-Dends were considered to be external tufted cells (n = 53 and n = 37, respectively).

A portion of the anatomically identified neurons was used for functional analysis. Because significant differences in eMRR widths and similarities could not be detected in the GL, the data from these three cell subtypes in the GL were combined and referred to as juxtaglomerular (JG) cells for functional comparisons. In the EPL, two types of cells were distinguished: cells with L-Dends and cells without L-Dends. The majority of these projection neurons in the EPL were considered to be middle tufted cells. For unclear reasons, odor-induced Ca^{2+} responses were only successfully recorded from cells with L-Dends. In the MCL, all of the labeled MCL cells had L-Dends. The majority of projection neurons in the MCL were considered to be mitral cells.

Wide-Field Imaging Analysis of Odor Response Patterns

Using heterozygous OMP-Synapto-pHluorin knockin mice (Bozza et al., 2004), olfactory sensory axon terminal glomerular activities were detected using a microscope (BX50WI; Olympus) that was equipped with a high speed CCD camera (NeuroCCD-SM256; Redshirt Imaging). The OB was illuminated with an LED light at 470 nm (M470L2, Thorlab). The excitation and emission lights were band-pass filtered with a GFP filter set (BrightLine GFP-4050A, Semrock) and collected at 25 Hz. Raw fluorescence traces from individual glomeruli were sampled by spatial averaging of 3–4 pixels that were located near the center of each glomerulus. Photobleaching was corrected by subtracting fluorescent responses observed during a no-odor imaging trial. Each series of images was evaluated by subtracting the resting fluorescence (F) (average of 75 images for 3 s prior to odorant delivery) and the resulting values were expressed as ΔF/F. Mann-Whitney tests were used to determine significant odor-evoked responses by comparing the averaged images before (for 3 s) and after odor onset (for 6 s). Differences of $p < 0.05$ were considered to be statistically significant. To compare the spatial activity patterns of glomeruli across animals, odorant-evoked activity patterns were aligned to landmarks, such as the sagittal sutures and the OB caudal sinuses. All spatial response maps were presented in pseudocolor.

Two-Photon Imaging

A customized Olympus two-photon imaging system was combined with the CCD imaging system, and a mode-locked pulse laser (Tsunami or MaiTai DeepSee, SpectraPhysics; 800–920 nm wavelength) was used for the two-photon fluorescent excitation. Three-dimensional images were captured in different focal planes at 5 μm intervals. Some of the glomerular modules (Figures 1D and 1E) and individual neurons (Figures S1C–S1E) were 3D reconstructed using Imaris software (Bitplane). Functional imaging recordings were performed at a speed of 1–3 frames/s. Off-line analysis was performed with Image-J software (NIH). Ca^{2+} responses were calculated as $\Delta F/F_0 = (F\text{-}F_0)/F_0$, where F_0 is the average baseline fluorescence observed before stimulation. Ca^{2+}responses to odor stimulation were performed at least four times during each recording. Excitatory/inhibitory Ca^{2+}responses were defined as significant average increases/decreases during the 6 s period after odor stimulation onset relative to the 3 s period before odor stimulation (Mann-Whitney test; $p < 0.05$ was considered to be statistically significant). The odorant selectivities of the neurons were summarized as excitatory and/or inhibitory molecular receptive ranges (eMRRs and iMRRs, respectively). The amplitudes of the odor-induced Ca^{2+} responses for each concentration were normalized to the strongest response to compare the odor sensitivities of each neuron. To compare the similarities between two labeled neurons, the number of odorants that excited both neurons were counted and divided by the total number of odorants that activated the neurons (Figures 6E, 7E, and 7F). The response similarity between two labeled neurons is also measured using a pair of vectors each of which represents response amplitudes of a neuron to the odorants. Pearson's correlation coefficient (Figures 7G and 7H) and a cosine of the angle between two vectors (cosine similarity; Figure S3) were used as the measures of similarity.

Statistical Analyses

Statistical analyses were performed using the Tukey-Kramer test for the data in Figure 2E; the Wilcoxon t test for the data in Figure 3G; the Steel-Dwass test for the data in Figures 4E and 6E; and t test of Pearson's correlation coefficient for the data in Figures 7E and 7F and S3. All values were expressed as mean ± the standard error of the mean (SEM), and $p < 0.05$ was considered significant.

SUPPLEMENTAL INFORMATION

Supplemental Information includes four figures, one table, and one movie and can be found with this article online at http://dx.doi.org/10.1016/j.neuron.2013.01.022.

ACKNOWLEDGMENTS

We thank Wei Chen for support, critical suggestions, and comments. We also thank Gordon M. Shepherd (Yale University) and Kensaku Mori (University of Tokyo) for comments on this manuscript. This work was supported by multiple NIH grants (DC010057 and DC009666 to S.N.; DC009853 to M.L.F.). S.K. was supported by multiple grants of the Japan Society for Promotion of Science (Institutional Program for Young Researcher Overseas Visits, and Young Investigator Grants [24791753]).

Accepted: January 16, 2013
Published: March 20, 2013

REFERENCES

Aungst, J.L., Heyward, P.M., Puche, A.C., Karnup, S.V., Hayar, A., Szabo, G., and Shipley, M.T. (2003). Centre-surround inhibition among olfactory bulb glomeruli. Nature *426*, 623–629.

Bozza, T., McGann, J.P., Mombaerts, P., and Wachowiak, M. (2004). In vivo imaging of neuronal activity by targeted expression of a genetically encoded probe in the mouse. Neuron *42*, 9–21.

Buck, L., and Axel, R. (1991). A novel multigene family may encode odorant receptors: a molecular basis for odor recognition. Cell *65*, 175–187.

Buonviso, N., Chaput, M.A., and Scott, J.W. (1991). Mitral cell-to-glomerulus connectivity: an HRP study of the orientation of mitral cell apical dendrites. J. Comp. Neurol. *307*, 57–64.

Buonviso, N., Chaput, M.A., and Berthommier, F. (1992). Temporal pattern analyses in pairs of neighboring mitral cells. J. Neurophysiol. *68*, 417–424.

Buonviso, N., Chaput, M.A., and Berthommier, F. (1996). Similarity of granular-induced inhibitory periods in pairs of neighboring mitral/tufted cells. J. Neurophysiol. *76*, 2393–2401.

Carey, R.M., and Wachowiak, M. (2011). Effect of sniffing on the temporal structure of mitral/tufted cell output from the olfactory bulb. J. Neurosci. *31*, 10615–10626.

Charpak, S., Mertz, J., Beaurepaire, E., Moreaux, L., and Delaney, K. (2001). Odor-evoked calcium signals in dendrites of rat mitral cells. Proc. Natl. Acad. Sci. USA *98*, 1230–1234.

Christie, J.M., Bark, C., Hormuzdi, S.G., Helbig, I., Monyer, H., and Westbrook, G.L. (2005). Connexin36 mediates spike synchrony in olfactory bulb glomeruli. Neuron *46*, 761–772.

Cury, K.M., and Uchida, N. (2010). Robust odor coding via inhalation-coupled transient activity in the mammalian olfactory bulb. Neuron *68*, 570–585.

Dhawale, A.K., Hagiwara, A., Bhalla, U.S., Murthy, V.N., and Albeanu, D.F. (2010). Non-redundant odor coding by sister mitral cells revealed by light addressable glomeruli in the mouse. Nat. Neurosci. *13*, 1404–1412.

Egaña, J.I., Aylwin, M.L., and Maldonado, P.E. (2005). Odor response properties of neighboring mitral/tufted cells in the rat olfactory bulb. Neuroscience *134*, 1069–1080.

Eyre, M.D., Antal, M., and Nusser, Z. (2008). Distinct deep short-axon cell subtypes of the main olfactory bulb provide novel intrabulbar and extrabulbar GABAergic connections. J. Neurosci. *28*, 8217–8229.

Ezeh, P.I., Wellis, D.P., and Scott, J.W. (1993). Organization of inhibition in the rat olfactory bulb external plexiform layer. J. Neurophysiol. *70*, 263–274.

Fukunaga, I., Berning, M., Kollo, M., Schmaltz, A., and Schaefer, A.T. (2012). Two distinct channels of olfactory bulb output. Neuron *75*, 320–329.

Grewe, B.F., Langer, D., Kasper, H., Kampa, B.M., and Helmchen, F. (2010). High-speed in vivo calcium imaging reveals neuronal network activity with near-millisecond precision. Nat. Methods *7*, 399–405.

Griff, E.R., Mafhouz, M., and Chaput, M.A. (2008). Comparison of identified mitral and tufted cells in freely breathing rats: II. Odor-evoked responses. Chem. Senses *33*, 793–802.

Hálasz, N., and Greer, C.A. (1993). Terminal arborizations of olfactory nerve fibers in the glomeruli of the olfactory bulb. J. Comp. Neurol. *337*, 307–316.

Hayar, A., Karnup, S., Shipley, M.T., and Ennis, M. (2004). Olfactory bulb glomeruli: external tufted cells intrinsically burst at theta frequency and are entrained by patterned olfactory input. J. Neurosci. *24*, 1190–1199.

Igarashi, K.M., Ieki, N., An, M., Yamaguchi, Y., Nagayama, S., Kobayakawa, K., Kobayakawa, R., Tanifuji, M., Sakano, H., Chen, W.R., and Mori, K. (2012). Parallel mitral and tufted cell pathways route distinct odor information to different targets in the olfactory cortex. J. Neurosci. *32*, 7970–7985.

Imamura, K., Mataga, N., and Mori, K. (1992). Coding of odor molecules by mitral/tufted cells in rabbit olfactory bulb. I. Aliphatic compounds. J. Neurophysiol. *68*, 1986–2002.

Imamura, F., Nagao, H., Naritsuka, H., Murata, Y., Taniguchi, H., and Mori, K. (2006). A leucine-rich repeat membrane protein, 5T4, is expressed by a subtype of granule cells with dendritic arbors in specific strata of the mouse olfactory bulb. J. Comp. Neurol. *495*, 754–768.

Jin, L., Han, Z., Platisa, J., Wooltorton, J.R., Cohen, L.B., and Pieribone, V.A. (2012). Single action potentials and subthreshold electrical events imaged in neurons with a fluorescent protein voltage probe. Neuron *75*, 779–785.

Kasowski, H.J., Kim, H., and Greer, C.A. (1999). Compartmental organization of the olfactory bulb glomerulus. J. Comp. Neurol. *407*, 261–274.

Kepecs, A., Uchida, N., and Mainen, Z.F. (2006). The sniff as a unit of olfactory processing. Chem. Senses *31*, 167–179.

Kim, D.H., Phillips, M.E., Chang, A.Y., Patel, H.K., Nguyen, K.T., and Willhite, D.C. (2011). Lateral connectivity in the olfactory bulb is sparse and segregated. Front. Neural Circuits *5*. http://dx.doi.org/10.3389/fncir.2011.00005.

Kiyokage, E., Pan, Y.Z., Shao, Z., Kobayashi, K., Szabo, G., Yanagawa, Y., Obata, K., Okano, H., Toida, K., Puche, A.C., and Shipley, M.T. (2010). Molecular identity of periglomerular and short axon cells. J. Neurosci. *30*, 1185–1196.

Kosaka, K., Toida, K., Aika, Y., and Kosaka, T. (1998). How simple is the organization of the olfactory glomerulus?: the heterogeneity of so-called periglomerular cells. Neurosci. Res. *30*, 101–110.

Linden, J.F., and Markram, H. (2003). Preface to the special issue. Cereb. Cortex *13*, 1.

Liu, S., and Shipley, M.T. (2008). Multiple conductances cooperatively regulate spontaneous bursting in mouse olfactory bulb external tufted cells. J. Neurosci. *28*, 1625–1639.

Lowe, G. (2002). Inhibition of backpropagating action potentials in mitral cell secondary dendrites. J. Neurophysiol. *88*, 64–85.

Ma, J., and Lowe, G. (2010). Correlated firing in tufted cells of mouse olfactory bulb. Neuroscience *169*, 1715–1738.

Macrides, F., Schoenfeld, T.A., Marchand, J.E., and Clancy, A.N. (1985). Evidence for morphologically, neurochemically and functionally heterogeneous classes of mitral and tufted cells in the olfactory bulb. Chem. Senses *10*, 175–202.

Mombaerts, P., Wang, F., Dulac, C., Chao, S.K., Nemes, A., Mendelsohn, M., Edmondson, J., and Axel, R. (1996). Visualizing an olfactory sensory map. Cell *87*, 675–686.

Mori, K., and Sakano, H. (2011). How is the olfactory map formed and interpreted in the mammalian brain? Annu. Rev. Neurosci. *34*, 467–499.

Mori, K., Kishi, K., and Ojima, H. (1983). Distribution of dendrites of mitral, displaced mitral, tufted, and granule cells in the rabbit olfactory bulb. J. Comp. Neurol. *219*, 339–355.

Mori, K., Mataga, N., and Imamura, K. (1992). Differential specificities of single mitral cells in rabbit olfactory bulb for a homologous series of fatty acid odor molecules. J. Neurophysiol. *67*, 786–789.

Mountcastle, V.B. (1997). The columnar organization of the neocortex. Brain *120*, 701–722.

Nagayama, S., Takahashi, Y.K., Yoshihara, Y., and Mori, K. (2004). Mitral and tufted cells differ in the decoding manner of odor maps in the rat olfactory bulb. J. Neurophysiol. *91*, 2532–2540.

Nagayama, S., Zeng, S., Xiong, W., Fletcher, M.L., Masurkar, A.V., Davis, D.J., Pieribone, V.A., and Chen, W.R. (2007). In vivo simultaneous tracing and $Ca^{(2+)}$ imaging of local neuronal circuits. Neuron *53*, 789–803.

Nagayama, S., Enerva, A., Fletcher, M.L., Masurkar, A.V., Igarashi, K.M., Mori, K., and Chen, W.R. (2010). Differential axonal projection of mitral and tufted cells in the mouse main olfactory system. Front. Neural Circuits *4*. http://dx.doi.org/10.3389/fncir.2010.00120.

Naritsuka, H., Sakai, K., Hashikawa, T., Mori, K., and Yamaguchi, M. (2009). Perisomatic-targeting granule cells in the mouse olfactory bulb. J. Comp. Neurol. *515*, 409–426.

Ohki, K., Chung, S., Ch'ng, Y.H., Kara, P., and Reid, R.C. (2005). Functional imaging with cellular resolution reveals precise micro-architecture in visual cortex. Nature *433*, 597–603.

Orona, E., Scott, J.W., and Rainer, E.C. (1983). Different granule cell populations innervate superficial and deep regions of the external plexiform layer in rat olfactory bulb. J. Comp. Neurol. *217*, 227–237.

Orona, E., Rainer, E.C., and Scott, J.W. (1984). Dendritic and axonal organization of mitral and tufted cells in the rat olfactory bulb. J. Comp. Neurol. *226*, 346–356.

Phillips, M.E., Sachdev, R.N., Willhite, D.C., and Shepherd, G.M. (2012). Respiration drives network activity and modulates synaptic and circuit processing of lateral inhibition in the olfactory bulb. J. Neurosci. *32*, 85–98.

Sachse, S., and Galizia, C.G. (2002). Role of inhibition for temporal and spatial odor representation in olfactory output neurons: a calcium imaging study. J. Neurophysiol. *87*, 1106–1117.

Schneider, S.P., and Scott, J.W. (1983). Orthodromic response properties of rat olfactory bulb mitral and tufted cells correlate with their projection patterns. J. Neurophysiol. *50*, 358–378.

Schoppa, N.E., and Westbrook, G.L. (2001). Glomerulus-specific synchronization of mitral cells in the olfactory bulb. Neuron *31*, 639–651.

Schoppa, N.E., and Westbrook, G.L. (2002). AMPA autoreceptors drive correlated spiking in olfactory bulb glomeruli. Nat. Neurosci. *5*, 1194–1202.

Shepherd, G.M., Chen, W.R., and Greer, C.A. (2004). Olfactory bulb. In The Synaptic Organization of the Brain, G.M. Shepherd, ed. (Oxford: Oxford University Press), pp. 165–216.

Shipley, M.T., and Ennis, M. (1996). Functional organization of olfactory system. J. Neurobiol. *30*, 123–176.

Shusterman, R., Smear, M.C., Koulakov, A.A., and Rinberg, D. (2011). Precise olfactory responses tile the sniff cycle. Nat. Neurosci. *14*, 1039–1044.

Smear, M., Shusterman, R., O'Connor, R., Bozza, T., and Rinberg, D. (2011). Perception of sniff phase in mouse olfaction. Nature *479*, 397–400.

Tan, J., Savigner, A., Ma, M., and Luo, M. (2010). Odor information processing by the olfactory bulb analyzed in gene-targeted mice. Neuron *65*, 912–926.

Uchida, N., Takahashi, Y.K., Tanifuji, M., and Mori, K. (2000). Odor maps in the mammalian olfactory bulb: domain organization and odorant structural features. Nat. Neurosci. *3*, 1035–1043.

Uchida, N., Kepecs, A., and Mainen, Z.F. (2006). Seeing at a glance, smelling in a whiff: rapid forms of perceptual decision making. Nat. Rev. Neurosci. *7*, 485–491.

Wachowiak, M. (2011). All in a sniff: olfaction as a model for active sensing. Neuron *71*, 962–973.

Wachowiak, M., and Cohen, L.B. (2001). Representation of odorants by receptor neuron input to the mouse olfactory bulb. Neuron *32*, 723–735.

Wachowiak, M., Denk, W., and Friedrich, R.W. (2004). Functional organization of sensory input to the olfactory bulb glomerulus analyzed by two-photon calcium imaging. Proc. Natl. Acad. Sci. USA *101*, 9097–9102.

Willhite, D.C., Nguyen, K.T., Masurkar, A.V., Greer, C.A., Shepherd, G.M., and Chen, W.R. (2006). Viral tracing identifies distributed columnar organization in the olfactory bulb. Proc. Natl. Acad. Sci. USA *103*, 12592–12597.

Yokoi, M., Mori, K., and Nakanishi, S. (1995). Refinement of odor molecule tuning by dendrodendritic synaptic inhibition in the olfactory bulb. Proc. Natl. Acad. Sci. USA *92*, 3371–3375.

Zeng, S., Lv, X., Zhan, C., Chen, W.R., Xiong, W., Jacques, S.L., and Luo, Q. (2006). Simultaneous compensation for spatial and temporal dispersion of acousto-optical deflectors for two-dimensional scanning with a single prism. Opt. Lett. *31*, 1091–1093.